The Astrophysical Journal, 860:137 (9pp), 2018 June 20 https://doi.org/10.3847/1538-4357/aac264

Constraints on Cosmological Parameters from the Angular Power Spectrum of a Combined 2500 deg^2 SPT-SZ and *Planck* Gravitational Lensing Map

G. Simard[1], Y. Omori[1,2,3], K. Aylor[4], E. J. Baxter[5,6,7], B. A. Benson[6,7,8], L. E. Bleem[6,9], J. E. Carlstrom[6,7,9,10,11], C. L. Chang[6,7,9], H-M. Cho[12], R. Chown[1], T. M. Crawford[6,7], A. T. Crites[6,7,13], T. de Haan[1,14], M. A. Dobbs[1,15], W. B. Everett[16], E. M. George[14,17], N. W. Halverson[16,18], N. L. Harrington[14], J. W. Henning[6,9], G. P. Holder[1,15,19,20], Z. Hou[6,7], W. L. Holzapfel[14], J. D. Hrubes[21], L. Knox[4], A. T. Lee[14,22], E. M. Leitch[6,7], D. Luong-Van[21], A. Manzotti[6,7], J. J. McMahon[23], S. S. Meyer[6,7,10,11], L. M. Mocanu[6,7], J. J. Mohr[24,25,26], T. Natoli[6,10,27], S. Padin[6,7], C. Pryke[28], C. L. Reichardt[14,29], J. E. Ruhl[30], J. T. Sayre[16,30], K. K. Schaffer[6,11,31], E. Shirokoff[6,7,14], Z. Staniszewski[30,32], A. A. Stark[33], K. T. Story[2,3,6,10], K. Vanderlinde[27,34], J. D. Vieira[19,20], R. Williamson[6,7], and W. L. K. Wu[6]

[1] Department of Physics and McGill Space Institute, McGill University, Montreal, Quebec H3A 2T8, Canada; gholder@illinois.edu
[2] Kavli Institute for Particle Astrophysics and Cosmology, Stanford University, 452 Lomita Mall, Stanford, CA 94305, USA
[3] Dept. of Physics, Stanford University, 382 Via Pueblo Mall, Stanford, CA 94305, USA
[4] Department of Physics, University of California, Davis, CA 95616, USA
[5] Center for Particle Cosmology, Department of Physics and Astronomy, University of Pennsylvania, Philadelphia, PA 19104, USA
[6] Kavli Institute for Cosmological Physics, University of Chicago, Chicago, IL 60637, USA
[7] Department of Astronomy and Astrophysics, University of Chicago, Chicago, IL 60637, USA
[8] Fermi National Accelerator Laboratory, MS209, P.O. Box 500, Batavia, IL 60510, USA
[9] High Energy Physics Division, Argonne National Laboratory, Argonne, IL 60439, USA
[10] Department of Physics, University of Chicago, Chicago, IL 60637, USA
[11] Enrico Fermi Institute, University of Chicago, Chicago, IL 60637, USA
[12] SLAC National Accelerator Laboratory, 2575 Sand Hill Road, Menlo Park, CA 94025, USA
[13] California Institute of Technology, Pasadena, CA 91125, USA
[14] Department of Physics, University of California, Berkeley, CA 94720, USA
[15] Canadian Institute for Advanced Research, CIFAR Program in Cosmology and Gravity, Toronto, ON, M5G 1Z8, Canada
[16] Center for Astrophysics and Space Astronomy, Department of Astrophysical and Planetary Sciences, University of Colorado, Boulder, CO 80309, USA
[17] European Southern Observatory, Karl-Schwarzschild-Straße 2, D-85748 Garching, Germany
[18] Department of Physics, University of Colorado, Boulder, CO 80309, USA
[19] Astronomy Department, University of Illinois at Urbana-Champaign, 1002 W. Green Street, Urbana, IL 61801, USA
[20] Department of Physics, University of Illinois Urbana-Champaign, 1110 W. Green Street, Urbana, IL 61801, USA
[21] University of Chicago, Chicago, IL 60637, USA
[22] Physics Division, Lawrence Berkeley National Laboratory, Berkeley, CA 94720, USA
[23] Department of Physics, University of Michigan, Ann Arbor, MI 48109, USA
[24] Faculty of Physics, Ludwig-Maximilians-Universität, D-81679 München, Germany
[25] Excellence Cluster Universe, D-85748 Garching, Germany
[26] Max-Planck-Institut für extraterrestrische Physik, D-85748 Garching, Germany
[27] Dunlap Institute for Astronomy & Astrophysics, University of Toronto, 50 St George St, Toronto, ON, M5S 3H4, Canada
[28] Department of Physics, University of Minnesota, Minneapolis, MN 55455, USA
[29] School of Physics, University of Melbourne, Parkville, VIC 3010, Australia
[30] Physics Department, Center for Education and Research in Cosmology and Astrophysics, Case Western Reserve University, Cleveland, OH 44106, USA
[31] Liberal Arts Department, School of the Art Institute of Chicago, Chicago, IL 60603, USA
[32] Jet Propulsion Laboratory, California Institute of Technology, Pasadena, CA 91109, USA
[33] Harvard-Smithsonian Center for Astrophysics, Cambridge, MA 02138, USA
[34] Department of Astronomy & Astrophysics, University of Toronto, 50 St George St, Toronto, ON, M5S 3H4, Canada
Received 2017 December 28; revised 2018 April 19; accepted 2018 May 1; published 2018 June 20

Abstract

We report constraints on cosmological parameters from the angular power spectrum of a cosmic microwave background (CMB) gravitational lensing potential map created using temperature data from 2500 deg^2 of South Pole Telescope (SPT) data supplemented with data from *Planck* in the same sky region, with the statistical power in the combined map primarily from the SPT data. We fit the lensing power spectrum to a model including cold dark matter and a cosmological constant (ΛCDM), and to models with single-parameter extensions to ΛCDM. We find constraints that are comparable to and consistent with those found using the full-sky *Planck* CMB lensing data, e.g., $\sigma_8\Omega_m^{0.25} = 0.598 \pm 0.024$ from the lensing data alone with weak priors placed on other parameters. Combining with primary CMB data, we explore single-parameter extensions to ΛCDM. We find $\Omega_k = -0.012^{+0.021}_{-0.023}$ or $M_\nu < 0.70$ eV at 95% confidence, in good agreement with results including the lensing potential as measured by *Planck*. We include two parameters that scale the effect of lensing on the CMB: A_L, which scales the lensing power spectrum in both the lens reconstruction power and in the smearing of the acoustic peaks, and $A^{\phi\phi}$, which scales only the amplitude of the lensing reconstruction power spectrum. We find $A^{\phi\phi} \times A_L = 1.01 \pm 0.08$ for the lensing map made from combined SPT and *Planck* data, indicating that the amount of lensing is in excellent agreement with expectations from the observed CMB angular power spectrum when not including the information from smearing of the acoustic peaks.

Key words: cosmic background radiation – cosmological parameters – gravitational lensing: weak

1. Introduction

Gravitational lensing of the cosmic microwave background (CMB) has emerged as a useful cosmological tool. CMB lensing, which probes all structure along a given line of sight, provides complementary information to the primary CMB fluctuations which measure structure at $z \sim 1100$. The sensitivity of CMB lensing peaks at intermediate redshifts ($z \sim 3$), making it complementary to large-scale structure surveys, the sensitivity of which typically peaks at lower redshifts, and with very different sources of possible systematic errors. Lensing of the CMB was first detected in cross-correlation with galaxies a decade ago (Smith et al. 2007); high signal-to-noise internal detections have now been achieved by many experiments (Das et al. 2011b; van Engelen et al. 2012; Planck Collaboration 2014b; POLARBEAR Collaboration 2014; BICEP2 Collaboration et al. 2016). For a review of CMB lensing, see Challinor & Lewis (2005).

The fluctuations in the CMB lensing potential form a nearly Gaussian projected field on the sky, with statistical properties determined by the geometry and the history of structure formation in the universe. Because the field is nearly Gaussian, essentially all the information is encoded in the angular power spectrum. The most precise CMB lensing power spectrum measurements to date are from the *Planck* experiment (Planck Collaboration 2016b).

Cosmological parameter fits that include CMB lensing information are broadly consistent with expectations from the primary CMB measurements alone (Planck Collaboration 2016a). There are, however, mild but interesting tensions ($\sim 2\sigma$) between constraints on cosmology from *Planck* primary CMB measurements and other cosmological probes. Specifically related to lensing, the amplitude of the matter power spectrum on galaxy scales (σ_8) inferred from *Planck* primary CMB data is slightly higher than that determined from cosmic shear measurements (Hildebrandt et al. 2017; Joudaki et al. 2017; Troxel et al. 2017). Further, specifically related to lensing of the CMB, the amount of lensing inferred from the measured smearing of the acoustic peaks is higher than that inferred from the direct measurement of the lensing-induced mode-coupling (Planck Collaboration 2016a). The amplitude of lensing is expected to be a powerful probe of neutrino masses (Abazajian et al. 2015), so discordance in measurements of lensing amplitudes is important for understanding the utility of these measurements as probes of particle physics.

This paper is a companion to Omori et al. (2017), referred to as O17 hereafter. In that work, we obtained a CMB temperature map by combining 150 GHz SPT and 143 GHz *Planck* data in the 2500 deg^2 South Pole Telescope (SPT)-SZ survey region, and we used the resulting temperature map to produce a map of the projected gravitational lensing potential. In this paper, we present a cosmological parameter analysis of the CMB lensing power spectrum derived in O17. This spectrum is shown in Figure 1, along with other recent measurements, including the full-sky *Planck* lensing power spectrum.

This work is divided as follows: in Section 2 we review gravitational lensing of the CMB and reconstruction of the lensing potential; in Section 3 we describe the CMB temperature data and simulations used for the O17 analysis and for this work; in Section 4 we describe how the lensing likelihood is constructed, including linear corrections for the unknown true CMB and lensing potential power spectra; in Section 5 we present the primary result of this paper: constraints on cosmological parameters; we close with a discussion.

Throughout this work, we use the *Planck* TT + LOWP + LENSING cosmology[35] (Planck Collaboration 2016a) as a fiducial model. This fiducial cosmology is used for generating the simulated data necessary for the lensing reconstruction. All CMB temperature and lensing potential power spectra used in the present analysis have been computed with the CAMB Boltzmann code[36] (Lewis et al. 2000).

2. Lensing Reconstruction Framework

In this section, we build the theoretical framework for the lensing likelihood, presenting selected elements from the lensing reconstruction pipeline. A more complete description of the procedure can be found in O17.

2.1. Lensing of CMB Temperature Fluctuations

Gravitational lensing remaps CMB fluctuations in position space (Lewis & Challinor 2006):

$$T^{\rm L}(\hat{\boldsymbol{n}}) = T^{\rm U}(\hat{\boldsymbol{n}} + \nabla\phi(\hat{\boldsymbol{n}})), \tag{1}$$

where $\phi(\hat{\boldsymbol{n}})$ is the projected gravitational lensing potential and superscripts L and U refer to the lensed and unlensed temperature fields respectively. To gain intuition, Equation (1) can be Taylor expanded as

$$T^{\rm L}(\hat{\boldsymbol{n}}) = T^{\rm U}(\hat{\boldsymbol{n}}) + \nabla T^{\rm U} \cdot \nabla\phi(\hat{\boldsymbol{n}}) + \ldots. \tag{2}$$

From the second term, it can be seen that the observed lensed temperature has a component that is the gradient of the unlensed field modulated by the lensing deflection $\nabla\phi$. If we transform to harmonic space, Equation (2) would have the second term on the right-hand side written as a weighted convolution of the temperature field and the lensing potential, where the harmonic transform for any particular mode for the lensed field could involve a sum over all of the modes of the unlensed field. Lensing thus introduces non-zero off-diagonal elements in the covariance of observed temperature fields in harmonic space (Okamoto & Hu 2003):

$$\Delta\langle T_{\ell_1 m_1} T_{\ell_2 m_2}\rangle = \sum_{LM} (-1)^M \begin{pmatrix} \ell_1 & \ell_2 & L \\ m_1 & m_2 & -M \end{pmatrix} W^{\phi}_{\ell_1\ell_2 L}\, \phi_{LM}, \tag{3}$$

where $T_{\ell m}$ are the spherical harmonic expansion coefficients of the temperature fields and ϕ_{LM} the coefficients of the projected lensing potential. The weight

$$W^{\phi}_{\ell_1\ell_2 L} = -\sqrt{\frac{(2\ell_1+1)(2\ell_2+1)(2L+1)}{4\pi}} \times C^{TT}_{\ell_1}\left(\frac{1+(-1)^{\ell_1+\ell_2+L}}{2}\right)\begin{pmatrix} \ell_1 & \ell_2 & L \\ 1 & 0 & -1 \end{pmatrix} \times \sqrt{L(L+1)\ell_1(\ell_1+1)} + (\ell_1 \leftrightarrow \ell_2) \tag{4}$$

characterizes the mode coupling induced by lensing (i.e., the effect of the convolution in Equation (2)).

[35] base_plikHM_TT_lowTEB_lensing.
[36] http://camb.info (2016 May version).

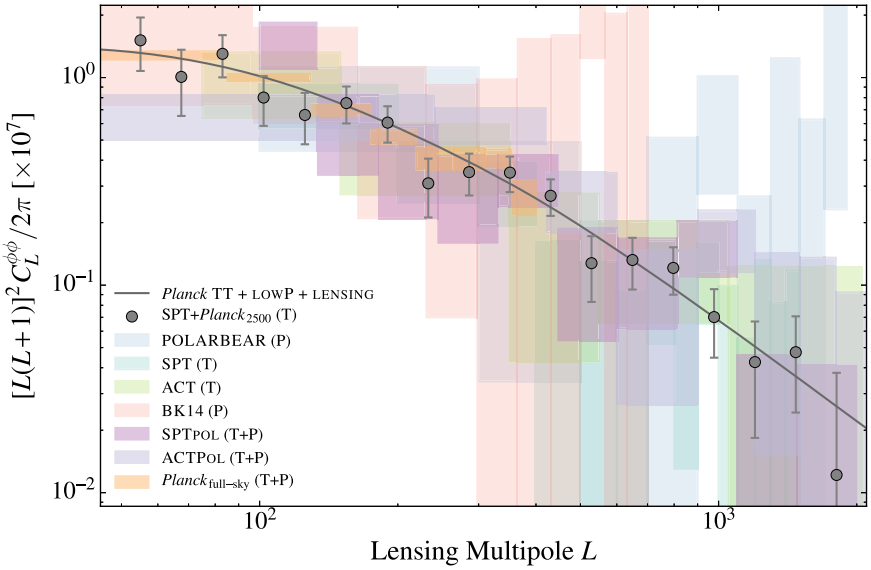

Figure 1. SPT + *Planck* lensing bandpowers from O17 along with earlier lensing estimates from the SPT-SZ survey (van Engelen et al. 2012) and recent lensing bandpowers obtained from temperature and polarization measurements from SPT$_{\rm POL}$ (Story et al. 2015). Also plotted are the most recent lensing autospectrum measurements from BICEP2+KECK ARRAY (BICEP2 Collaboration et al. 2016), *Planck* (Planck Collaboration 2016b), POLARBEAR (POLARBEAR Collaboration 2014) and ACT$_{\rm POL}$ (Sherwin et al. 2017), and a prediction for the lensing power spectrum using the best-fit cosmological parameters from the *Planck* TT + LOWP + LENSING cosmology (Planck Collaboration 2016a).

2.2. Lensing Map Reconstruction

The lensing potential can be estimated from observed CMB maps by measuring the lensing-induced mode coupling of Equation (3) between pairs of modes in the observed temperature field (Zaldarriaga & Seljak 1999; Hu & Okamoto 2002). In general, it is best to use pairs in harmonic space that have good signal-to-noise for measuring lensing. For this purpose, it is useful to work with a filtered map: $\bar{T}_{\ell m} \equiv F_{\ell m} T_{\ell m}$, with the filter $F_{\ell m} \equiv (C_\ell + N_{\ell m})^{-1}$ for a given CMB power spectrum C_ℓ and an anisotropic (m-dependent) noise power spectrum $N_{\ell m}$.

A formally optimal estimator (at first order) which maximizes signal to noise in the estimated lensing potential (Hu & Okamoto 2002) is

$$\bar{\phi}_{LM} = \frac{(-1)^M}{2} \sum_{\substack{\ell_1, m_1 \\ \ell_2, m_2}} \begin{pmatrix} \ell_1 & \ell_2 & L \\ m_1 & m_2 & -M \end{pmatrix} W^{\phi}_{\ell_1 \ell_2 L}\, \bar{T}_{\ell_1 m_1} \bar{T}_{\ell_2 m_2}. \quad (5)$$

We use Equation (5) as our ϕ estimator for this analysis. There are other choices (e.g., Namikawa et al. 2013) for how to weight the mode pairs that sacrifice some signal-to-noise but reduce foreground contamination. Lensing reconstruction is done with the QUICKLENS code.[37]

The relationship between the filtered estimate of the lensing potential resulting from Equation (5) and the true potential can be written as

$$\bar{\phi}_{LM} \equiv \mathcal{R}^{\phi}_{LM} \phi_{LM}, \quad (6)$$

defining a response function $\mathcal{R}_{LM}$ that in general depends on both L and M. As outlined in O17, this response function has been calibrated using simulations. We estimate it by measuring the cross-spectrum of simulated lensing potential outputs with the input lensing potential maps and normalizing by the autospectrum of the inputs.

The true amplitude of mode coupling in the CMB temperature field induced by lensing is sensitive to the true (unknown) temperature power spectrum, as can be seen in Equations (3) and (4). What is measured in the data is some amount of mode coupling; to turn this into an estimate of the amplitude of the lensing potential, an assumption is made about the typical amplitudes of the modes being coupled. The response function thus depends on the assumed cosmological parameters. To explore this cosmological dependence, we use an isotropic approximation to the full anisotropic response function and its dependence on cosmology. In the case where both the signal and noise are isotropic (i.e., the CMB signal and noise only depend statistically on ℓ and not m), the response function can be written as

$$\mathcal{R}^{\phi}_{L} = \frac{1}{2L+1} \sum_{\ell_1, \ell_2} W^{\phi, t}_{\ell_1 \ell_2 L} W^{\phi, f}_{\ell_1 \ell_2 L} F_{\ell_1} F_{\ell_2}, \quad (7)$$

where we have indicated extra superscripts on the weight functions for either the true amount of mode coupling (t) or the assumed amount for our fiducial cosmology (f). The filters F_ℓ are calculated for the fiducial cosmology. We use Equation (7) and its dependence on cosmology to determine the cosmology-dependent corrections to the simulation-based response function.

The survey mask, point source mask, and spatially varying noise all violate statistical stationarity in the data, and consequently they introduce mode coupling that can bias the lensing reconstruction. The result is that the lensing reconstruction has a non-zero mean signal—even in the absence of true lensing signal—that depends on the survey geometry, mask, and noise properties. This mean field $\bar{\phi}^{\rm MF}_{LM}$ is calculated using simulations and removed.

[37] http://github.com/dhanson/quicklens

After removing the mean field and correcting for the response function, the final estimate of the lensing potential is

$$\hat{\phi}_{LM} = \frac{\bar{\phi}_{LM} - \bar{\phi}^{\rm MF}_{LM}}{\mathcal{R}^{\phi}_{LM}}. \quad (8)$$

2.3. Lensing Autospectrum Estimation

To estimate the angular power spectrum of the CMB lensing map obtained in the previous section, we multiply the estimate $\hat{\phi}$ by the survey mask (including point source and galaxy cluster masking) and use `PolSpice`[38] (Szapudi et al. 2001; Chon et al. 2004) to compute the spectrum of the masked map.

The resulting power spectrum is a biased estimate of the true lensing power spectrum. Known sources of bias include a straightforward noise bias, $N_L^{(0)}$, that comes from taking an autospectrum of data with noise in it (where "noise" here includes the Gaussian part of the CMB temperature field and any other sky signal), and a bias that arises from ambiguity in exactly which lensing modes are being measured in the power spectrum, $N_L^{(1)}$ (Kesden et al. 2003). The superscript denotes the order of the lensing power spectrum involved: $N_L^{(0)}$ is independent of the true lensing power and only depends on the instrument noise and sky power, while $N_L^{(1)}$ has a linear dependence on the lensing power. As detailed in O17, we calculate these biases using simulations and subtract them from the measured power spectrum

$$\hat{C}_L^{\phi\phi} = C_L^{\hat{\phi}\hat{\phi}} - N_L^{(0)} - N_L^{(1)}. \quad (9)$$

We use a realization-dependent $N_L^{(0)}$ estimate that takes into account the power in the particular realization but does not depend on the assumed cosmology (Namikawa et al. 2013).

The $N_L^{(1)}$ bias depends linearly on the lensing power and will therefore depend on cosmological parameters. In the flat-sky limit (Kesden et al. 2003; Das et al. 2011b; Planck Collaboration 2014b) and assuming isotropic noise and filtering, the bias is

$$\begin{aligned} N_L^{(1)} = & \frac{1}{\mathcal{R}^{\phi}_L \mathcal{R}^{\phi}_L} \int \frac{d^2\ell_1}{(2\pi)^2} \int \frac{d^2\ell_3}{(2\pi)^2} \\ & \times F_{\ell_1} F_{\ell_2} F_{\ell_3} F_{\ell_4} W^{\phi,f}(\ell_1, \ell_2) W^{\phi,f}(\ell_3, \ell_4) \\ & \times [C^{\phi\phi}_{|\ell_1-\ell_3|} W^{\phi,t}(-\ell_1, \ell_3)\, W^{\phi,t}(-\ell_2, \ell_4) \\ & + C^{\phi\phi}_{|\ell_1-\ell_4|} W^{\phi,t}(-\ell_1, \ell_4)\, W^{\phi,t}(-\ell_2, \ell_3)], \end{aligned} \quad (10)$$

where the weight $W^{\phi}(\ell_1, \ell_2)$ is the flat-sky version of Equation (4).

There is a dependence on both the true CMB power (just as for $\mathcal{R}^{\phi}_L$) and the lensing power. To explore this cosmological dependence (below), we will use Equation (10) to determine the cosmology-dependent corrections to the $N_L^{(1)}$ that is derived from simulations.

The next-order $N_L^{(2)}$ bias is largely removed by using the lensed theory temperature power spectrum rather than the unlensed spectrum when constructing the lensing estimator (Hanson et al. 2011). There are other biases, such as the $N_L^{(3/2)}$ bias (Böhm et al. 2016), which are small at the precision of the current work, and will be neglected.

We estimate uncertainties on the lensing power spectrum by averaging over $N_s = 198$ simulations:

$$(\Delta\hat{C}_L^{\phi\phi})^2 = \frac{1}{N_s - 1} \sum_{i=1}^{N_s} (\hat{C}^{\phi\phi}_{L;i} - \langle \hat{C}_L^{\phi\phi} \rangle_{N_s})^2. \quad (11)$$

This procedure could be used to generate a full covariance matrix, but for this analysis we assume that uncertainties are uncorrelated between bins. This is expected for the relatively large bins that we use and the realization-dependent removal of the $N_L^{(0)}$ bias that strongly reduces the off-diagonal elements of the covariance matrix (Schmittfull et al. 2013). From simulations, we measured the correlation between bins to be no more than 5%.

3. Lensing Data

The binned CMB lensing angular power spectrum (or "lensing bandpowers") $\hat{C}^{\phi\phi}_{L_b}$ computed in O17, using the methods described in that work and summarized in the previous section, is shown in Figure 1 (along with other recent measurements from the literature), and the bin ranges and bandpower values and uncertainties are listed in Table 1.[39] We will hereafter refer to this as the "SPT + *Planck*" lensing measurement.

The higher angular resolution of the SPT greatly increases the lensing signal-to-noise per pixel over *Planck* from the larger number of available small-scale modes which can be used for measuring the lensing-induced mode coupling. Combining the *Planck* and SPT temperature maps strongly reduces the uncertainties, in particular on small scales (higher L) as compared to using only the SPT data. This happens because the lensing map only uses modes in the temperature map extending to $\ell = 3000$, to minimize possible foreground contamination. The high-L lensing modes require probing correlations in the temperature angular modes that are widely separated in harmonic space. By using the *Planck* data to recover the low-ℓ modes, there is an increased number of large-separation mode pairs.

As shown in O17, the SPT + *Planck* measurements over the 2500 deg^2 SPT-SZ survey area are more precise than the *Planck*-only full-sky constraints for $L \gtrsim 1000$. From the relative sky coverage, the *Planck*-only uncertainties using only the SPT region would be more than three times larger than the *Planck*-only full-sky constraints. The combined SPT + *Planck* measurements are thus nearly statistically independent, adding substantial new information.

Small-scale lensing measurements are most susceptible to foreground contamination, as shown in van Engelen et al. (2014). In that work, it was found that foreground contamination increased dramatically beyond $L \sim 2000$ for CMB map filtering choices similar to those adopted in O17. For the cosmological parameter estimation in this work, we therefore use the SPT + *Planck* lensing measurements only below $L = 2000$.

A comparison of the O17 bandpowers with the prediction from the best-fit *Planck* cosmology is shown in Figure 2. The ratio is shown with and without a correction for foreground contamination, based on van Engelen et al. (2014). The estimated contamination is small, never exceeding more than 5% of the uncertainty in any L bin, but not completely

[38] http://www2.iap.fr/users/hivon/software/PolSpice

[39] https://pole.uchicago.edu/public/data/simard18

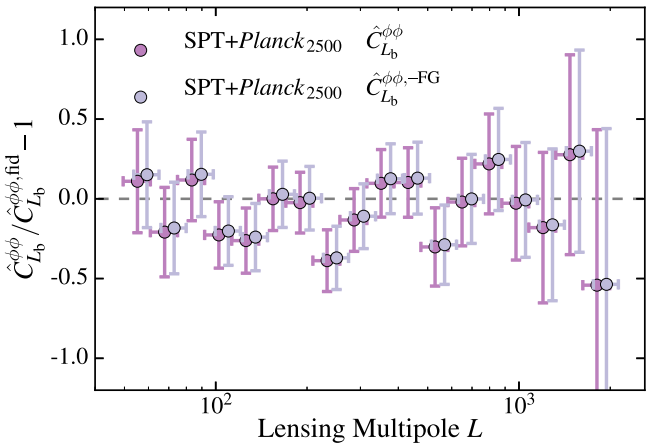

Figure 2. Ratio of lensing bandpowers to lensing power spectrum predicted for the best-fit *Planck* 2015 cosmological parameters. Shown are both the raw lensing bandpowers and the results after subtracting the best estimate of foreground contamination.

Table 1
Foreground-removed Lensing Bandpowers Used in This Analysis

L	$[L_b(L_b+1)]^2\,\hat{C}^{\phi\phi}_{L_b}/2\pi$ $[\times 10^7]$
50–60	1.51 ± 0.44
61–74	1.01 ± 0.35
75–91	1.30 ± 0.30
92–112	0.80 ± 0.22
113–138	0.66 ± 0.18
139–170	0.75 ± 0.15
171–209	0.61 ± 0.12
210–256	0.309 ± 0.098
257–315	0.350 ± 0.080
316–386	0.348 ± 0.068
387–474	0.269 ± 0.054
475–582	0.128 ± 0.045
583–715	0.132 ± 0.037
716–877	0.121 ± 0.031
878–1077	0.070 ± 0.025
1078–1322	0.043 ± 0.024
1323–1622	0.048 ± 0.023
1623–1991	0.012 ± 0.026

negligible. The uncertainty in the template is fractionally roughly 30% of the template amplitude at low L; the uncertainty in the template in any bin is <2% of the lensing bandpower uncertainty. The O17 bandpowers are consistent with expectations from *Planck*, with O17 finding a relative amplitude of 0.95 ± 0.06 for the best-fit *Planck* TT + LOWP + LENSING cosmology.

In the likelihood analysis described in the following section, the theory model includes this mean foreground contamination, as well as a term in the covariance to account for uncertainty in the foreground level.

4. Lensing Likelihood

In this section, we describe how we obtain the lensing likelihood function for the SPT + *Planck* lensing data as a function of cosmological parameters, $\ln\mathcal{L}(\boldsymbol{\Theta})$:

$$-2\ln\mathcal{L}(\boldsymbol{\Theta}) = \sum_{i,j}[\hat{C}^{\phi\phi}_{L^i_b} - C^{\phi\phi,\mathrm{th}}_{L^i_b}(\boldsymbol{\Theta})]\,\mathbb{C}^{-1}_{L^i_b L^j_b}[\hat{C}^{\phi\phi}_{L^j_b} - C^{\phi\phi,\mathrm{th}}_{L^j_b}(\boldsymbol{\Theta})]. \quad (12)$$

We make the approximation that the reconstructed lensing bandpowers $\hat{C}^{\phi\phi}_{L_b}$ are Gaussian-distributed and uncorrelated between bins, but that there is correlation between bins coming from the uncertainty in the foreground subtraction. We assume that the uncertainty in the residual foreground as reported in van Engelen et al. (2014) is completely correlated between bins, leading to off-diagonal terms in the covariance matrix. The $C^{\phi\phi,\mathrm{th}}_{L_b}(\boldsymbol{\Theta})$ bandpowers correspond to the binned theory lensing power spectrum at a given cosmology $\boldsymbol{\Theta}$, with the foreground template added.

4.1. Linear Corrections

The choice of cosmological model affects the computation of the estimated lensing bandpowers through the calculation of the response function and through the calculation of the $N^{(1)}_L$ bias term. These effects need to be included in the likelihood analysis.

The response function $\mathcal{R}^{\phi}_{LM}$ and $N^{(1)}_L$ correction for the fiducial cosmology are obtained using simulations and calculated using two-dimensional, anisotropic weighting. To calculate the cosmological corrections to these terms, we use isotropic approximations to both the response function and the $N^{(1)}_L$ bias (see Equations (7) and (10)). Within the range of allowed parameters, the cosmological corrections are relatively small, and we expect the error on these corrections from using the isotropic approximation to be negligible.

At a given point in parameter space, we apply the cosmology-dependent response function and $N^{(1)}_L$ corrections to the theory spectrum (Planck Collaboration 2016b):

$$C^{\phi\phi,\mathrm{th}}_L = \frac{(\mathcal{R}^{\phi}_L)^2|_\Theta}{(\mathcal{R}^{\phi}_L)^2|_f} C^{\phi\phi,\mathrm{th}}_L|_\Theta + N^{(1)}_L|_\Theta - N^{(1)}_L|_f. \quad (13)$$

To obtain these corrections, we use a linear approximation, Taylor-expanding around the response function or $N^{(1)}_L$ bias calculated for the fiducial cosmology. For a temperature or lensing power spectrum that differs by Δ from the fiducial spectrum, we obtain:

$$\Delta(\mathcal{R}^{\phi}_L)^2|_\Theta \simeq M^{(R)}_{L,\ell'}|_f \times \Delta C^{TT}_{\ell'}|_\Theta, \quad (14)$$

where $M^{(R)}_{L,\ell'} \equiv \frac{C^{\phi\phi}_L}{(\mathcal{R}^{\phi}_L)^2}\frac{\partial(\mathcal{R}^{\phi}_L)^2}{\partial C^{TT}_{\ell'}}$, and

$$\Delta N^{(1)}_L|_\Theta \simeq M^{(1)}_{L,L'}|_{\mathrm{fid}} \times \Delta C^{\phi\phi}_{L'}|_\Theta, \quad (15)$$

where $M^{(1)}_{L,L'} \equiv \frac{\partial N^{(1)}_L}{\partial C^{\phi\phi}_{L'}}$. The matrices M were calculated using binned versions of the temperature and lensing power spectra. In principle there is also a dependence on the temperature power spectrum in the $N^{(1)}_L$ correction, but that term was found to be negligible.

5. Constraints on Cosmological Parameters

Sourced mainly by potential wells at intermediate redshifts, gravitational lensing of the CMB can constrain late-time cosmological parameters affecting the growth of structure and the expansion of the universe, such as neutrino masses (Smith et al. 2006; Abazajian et al. 2015), and as a geometrical effect it can constrain curvature (Sherwin et al. 2011). Because of the combined sensitivity to the geometry and the growth of structure, lensing can break degeneracies between

cosmological parameters constrained by the CMB alone, including the angular diameter distance degeneracy (Stompor & Efstathiou 1999).

Recent detections of CMB lensing have proven its significance as a cosmological probe, on its own or in combination with CMB temperature and polarization measurements (Das et al. 2011b; van Engelen et al. 2012; Planck Collaboration 2014b, 2016b). In the following section, we show the most significant improvements on cosmological parameters constraints provided by the SPT + *Planck* lensing measurements over 2500 deg^2 as compared to the full-sky *Planck* primary CMB measurements on their own.

To determine the posterior probability distributions of the cosmological parameters from SPT + *Planck* lensing data in combination with CMB data, we use Markov chain Monte Carlo (MCMC) methods (Christensen et al. 2001) through the publicly available COSMOMC[40] package (Lewis & Bridle 2002).

Assuming a spatially flat universe, the properties of a Λ cold dark matter (ΛCDM) model can be represented by the following six parameters, which are the base set of parameters to be varied in the chains: the baryon density $\Omega_b h^2$, the cold dark matter density $\Omega_c h^2$, the optical depth at reionization τ, the angular scale of the sound horizon at the surface of last scattering θ_s, the amplitude A_s, and power-law spectral index n_s of primordial scalar perturbations, both taken at a pivot scale of $k = 0.05\,\mathrm{Mpc}^{-1}$ as chosen in the cosmological parameters analysis of Planck Collaboration (2014a). We will often use parameters derived from these six, including the total matter density Ω_m.

For constraints based only on lensing, the same priors as in Sherwin et al. (2017) have been applied. When computing constraints combining CMB lensing measurements with primary CMB measurements, the *Planck* TT and lowP likelihoods have been used, the latter relying on low ℓ CMB temperature and polarization data.

5.1. ΛCDM Model

An alternative way to parameterize the amplitude of the matter power spectrum is σ_8, the rms mass fluctuation today in 8 h^{-1} Mpc spheres assuming linear theory. This parameter is convenient for comparisons with results from galaxy surveys.

In Figure 3, constraints from lensing experiments, both CMB lensing (Planck Collaboration 2016b; Sherwin et al. 2017) and cosmic shear (Hildebrandt et al. 2017; Joudaki et al. 2017; Troxel et al. 2017), are shown in the $\sigma_8 - \Omega_\mathrm{m}$ plane, compared with expectations from the primary CMB fluctuations as measured by *Planck*. There have been hints of mild tension between *Planck* CMB power spectrum constraints and probes of low-redshift structure. The CMB lensing constraints are all highly consistent with each other, and it can be seen that the constraints from this paper (the SPT + *Planck* CMB lensing data) overlap with both the low-redshift probes and the primary CMB estimates, although the primary CMB data are substantially more precise. In making the CMB-lensing-only constraints, as was done in Planck Collaboration (2016b) and Sherwin et al. (2017), the corrections to the response function were held at the best-fit cosmology corresponding to the *Planck* TT and lowP likelihoods[41] (Planck Collaboration 2016a). The close agreement between SPT + *Planck* and *Planck* is not simply from the combined SPT + *Planck* data set including data from *Planck*. The SPT + *Planck* data are based on only ~2500 deg^2, and are mainly driven by the SPT data.

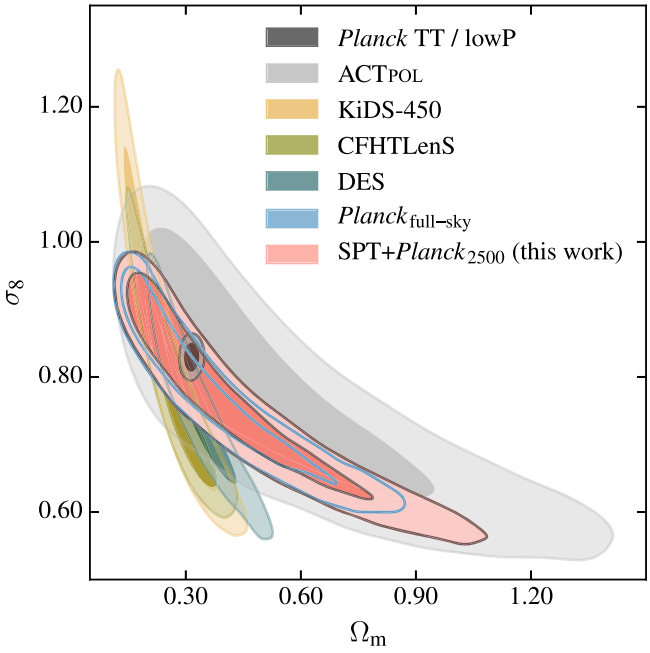

Figure 3. Lensing constraints on σ_8 and Ω_m from optical surveys (KiDS-450, CFHTLens, DES) and CMB measurements (ACT$_\mathrm{POL}$, *Planck* full sky, SPT + *Planck* 2500 deg^2). Also shown are constraints from the *Planck* primary CMB power spectra. This work is in good agreement with both CMB and optical surveys.

Joint constraints on Ω_m and σ_8 obtained by combining the CMB lensing data with the primary CMB measurements from *Planck* are shown in Figure 4. In general, the CMB lensing data (either the full-sky *Planck* or 2500 deg^2 SPT + *Planck*) prefer lower values of σ_8, as could be expected from Figure 3. A commonly used parameter for lensing constraints is $\sigma_8\Omega_\mathrm{m}^{0.25}$. For SPT + *Planck* we find $\sigma_8\Omega_\mathrm{m}^{0.25} = 0.598 \pm 0.024$, in excellent agreement with both the value found using the *Planck* full-sky lensing reconstruction, 0.591 ± 0.021 (Planck Collaboration 2016b), and the estimate by ACT$_\mathrm{POL}$ of 0.643 ± 0.054 (Sherwin et al. 2017).

CMB lensing data are most sensitive to overall shifts in the amplitude of matter fluctuations. This amplitude can be expressed as the rms deflection angle $\langle d^2\rangle^{1/2}$. For SPT + *Planck*, we use the samples from the MCMC chains for ΛCDM to determine that this rms deflection angle is 2.27 ± 0.16 arcmin (68%), in good agreement with the extremely precise measurement of the full-sky *Planck* survey of 2.46 ± 0.06.

5.2. Lensing Amplitude Compared to Expectations

Gravitational lensing of the CMB leads to a small amount of smearing of the acoustic oscillations in the primary fluctuations, an effect that has been well measured (Das et al. 2011a; Keisler et al. 2011). The primary CMB fluctuations as observed by *Planck* show weak evidence for a slightly elevated amount of lensing-like smearing of the acoustic peaks, although the lensing power directly measured by *Planck* shows no such excess (Planck Collaboration 2016b). Using the same effect in SPT temperature (Story et al. 2013) and polarization (Henning et al. 2017) power spectra, there was no evidence

[40] http://cosmologist.info/cosmomc/(2016 July version).
[41] base_plikHM_TT_lowTEB.

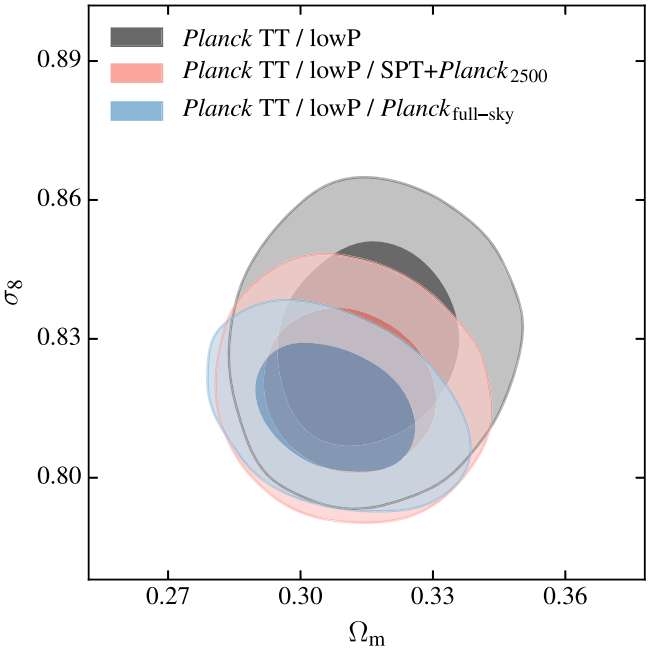

Figure 4. Constraints on σ_8 and Ω_m, combining CMB lensing data with primary CMB constraints. The largest contours show CMB primary CMB constraints from *Planck*, intermediate contours show the impact of adding the 2500 deg^2 SPT + *Planck* data, and the smallest contours show *Planck* primary data combined with *Planck* full-sky lensing results. This work is in excellent agreement with the *Planck* full-sky lensing result.

for such an excess of peak smoothing, with a modest ($\sim 1\sigma$) preference for less lensing than expected.

The expected amount of lensing depends on the somewhat uncertain cosmological parameters. To explore this, we marginalize over cosmological parameters and use new parameters to artificially scale the amount of lensing: A_L scales the lensing power spectrum in both the lens reconstruction power and in the smearing of the acoustic peaks, and $A^{\phi\phi}$ scales only the amplitude of the CMB lensing reconstruction power spectrum. This parameterization ensures that the ΛCDM parameters that control the predicted degree of lensing (such as $\Omega_b h^2$ and σ_8) are determined without considering the measured amount of peak smearing or mode coupling, and that these measurements are reflected entirely in A_L and $A^{\phi\phi}$.

As these parameters are defined, the ΛCDM prediction for the reconstructed lensing power spectrum gets multiplied by both A_L and $A^{\phi\phi}$. Therefore, the combination $A^{\phi\phi} \times A_L$ represents the amplitude for the lensing power relative to the ΛCDM prediction when the cosmological parameter fits are not sensitive to the observed amount of peak smearing.

With A_L fixed to unity the known preference in the *Planck* primary data for $A_L > 1$ will instead drive a preference for models with higher intrinsic lensing amplitudes, leading to a preference for lower values of $A^{\phi\phi}$ when compared with lensing reconstruction measurements that are otherwise consistent with ΛCDM. When A_L is free, the peak-smoothing preference for $A_L > 1$ increases the predicted lensing reconstruction power and therefore causes a lower $A^{\phi\phi}$ for a given model compared with the lensing power spectrum measurement. The combination $A_L \times A^{\phi\phi}$ thus gives the amplitude of the lensing power spectrum compared to *Planck*-allowed ΛCDM predictions when the peak smoothing effect is not reflected in the *Planck* constraints.

Posterior distributions for A_L, $A^{\phi\phi}$, and $A^{\phi\phi} \times A_L$ from chains using combinations of *Planck* primary CMB data, the *Planck* lensing power spectrum, and the lensing power spectrum in this work are shown in Figure 5. For models with $A_L = 1$ the measured SPT + *Planck* lensing power spectrum is somewhat low, with $A^{\phi\phi} = 0.91 \pm 0.06$. The CMB lensing reconstruction power spectrum measurements show no evidence for an anomalous amount of lensing relative to the amount predicted from the best-fit ΛCDM parameters determined in the primary CMB data when the peak smearing effect has been marginalized over. Using SPT + *Planck* data, we find $A^{\phi\phi} \times A_L = 1.01 \pm 0.08$ relative to the predicted level of lensing for ΛCDM marginalized over A_L; using the full-sky *Planck* full-sky lensing reconstruction, the result is only slightly higher, $A^{\phi\phi} \times A_L = 1.05 \pm 0.06$. The peak smearing in the *Planck* primary CMB power spectra, meanwhile, indicates mild evidence for enhanced lensing, with $A_L = 1.22 \pm 0.10$.

5.3. Spatial Curvature

Inflationary models predict that the universe should be close to spatially flat, and the combination of observations of the primary CMB, supernovae Ia, baryon acoustic oscillations, and local Hubble constant measurements shows that spatial curvature is not large (e.g., Komatsu et al. 2011). Constraints from the primary CMB have a geometrical degeneracy that allows spatial curvature to be increased while the Hubble constant is adjusted to keep the angular diameter distance to last scattering fixed; as a result, CMB measurements have historically relied on Hubble constant priors or external measurements to constrain curvature. As a probe of the local universe, lensing partially lifts this degeneracy (Sherwin et al. 2011). Figure 6 demonstrates this degeneracy-breaking by adding 2500 deg^2 SPT + *Planck* or *Planck* full-sky lensing reconstruction information to the *Planck* primary CMB measurements. The constraint on spatial curvature from adding SPT + *Planck* lensing information to *Planck* primary CMB is $\Omega_k = -0.012^{+0.021}_{-0.023}$ at 95% confidence.

5.4. Massive Neutrinos

CMB lensing, as a measurement of the amplitude of clustering at intermediate redshifts, is a potentially powerful probe of neutrino masses (Smith et al. 2006; Abazajian et al. 2015). Neutrino oscillation experiments have precisely measured the differences in the squares of the masses between the neutrino eigenstates, but the absolute masses have not been measured. Laboratory limits constrain the mass of the electron neutrino, but the strongest constraints on absolute neutrino masses currently come from cosmology. Having a substantial amount of the energy density in the form of massive neutrinos leads to a suppression of structure on small scales in the matter power spectrum. The *Planck* primary CMB measurements limit the sum of the masses to be $M_\nu < 0.72$ eV at 95% confidence (Planck Collaboration 2016a). This constraint is strongly driven by the measurement of lensing through the smearing of peaks in the CMB power spectra.

As was seen in Planck Collaboration (2016a), Figure 7 shows that adding information from the lensing reconstruction power spectrum reduces the M_ν posterior value at zero, but the lensing reconstruction data also rule out large values of M_ν, with the combined result being a similar 95% upper limit.

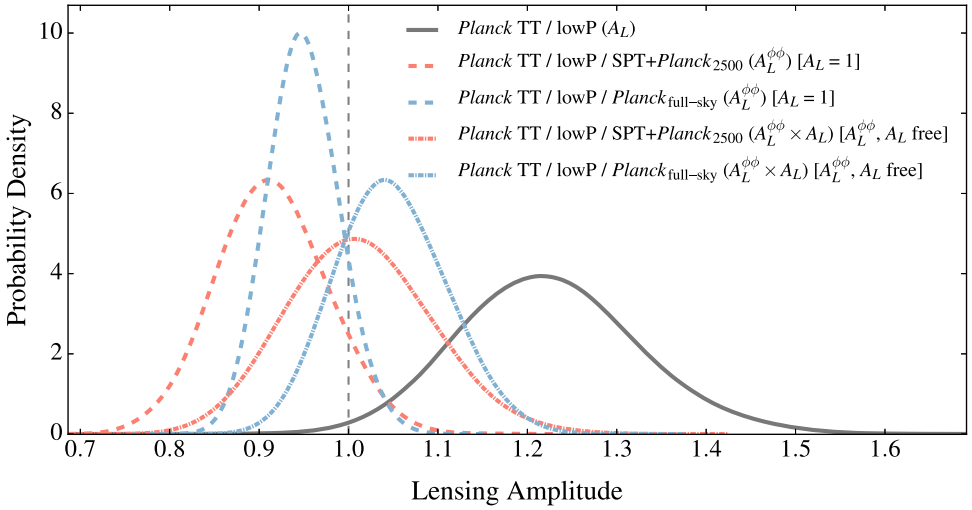

Figure 5. Lensing amplitude constraints. The solid line shows the marginalized posterior distribution of A_L from a fit using only *Planck* primary CMB power spectrum data. This is a measure of the level of smearing of the acoustic peaks relative to the prediction for ΛCDM cosmological parameters from the *Planck* power spectrum, ignoring the peak smearing information. Dashed lines show posterior distributions for $A^{\phi\phi}$ from fits to *Planck* power spectrum and full-sky *Planck* or 2500 deg^2 SPT + *Planck* lensing reconstruction data in which only the lensing reconstruction power spectrum is allowed to vary, and the peak smearing is constrained to be that expected for ΛCDM. This is a measure of the lensing reconstruction amplitude relative to the prediction for ΛCDM cosmological parameters from the *Planck* power spectrum including the peak smearing information. Finally, the dotted–dashed lines show posterior distributions for $A^{\phi\phi} \times A_L$, i.e., the lensing reconstruction amplitude relative to predictions for ΛCDM cosmological parameters from the *Planck* power spectrum, ignoring the peak smearing information, from a fit in which $A^{\phi\phi}$ and A_L are allowed to vary.

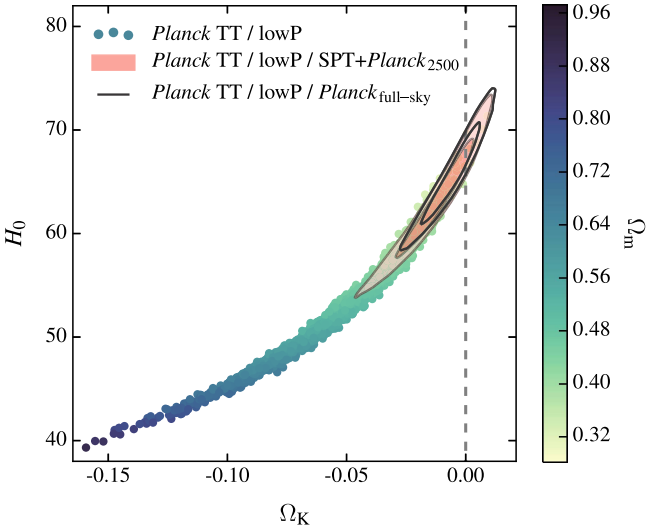

Figure 6. Constraints on curvature for *Planck* primary CMB power spectra alone (colored points), and adding either full-sky *Planck* lensing (black contours) or 2500 deg^2 SPT + *Planck* lensing data (green). Points from the no-lensing chain are color-coded by the matter density.

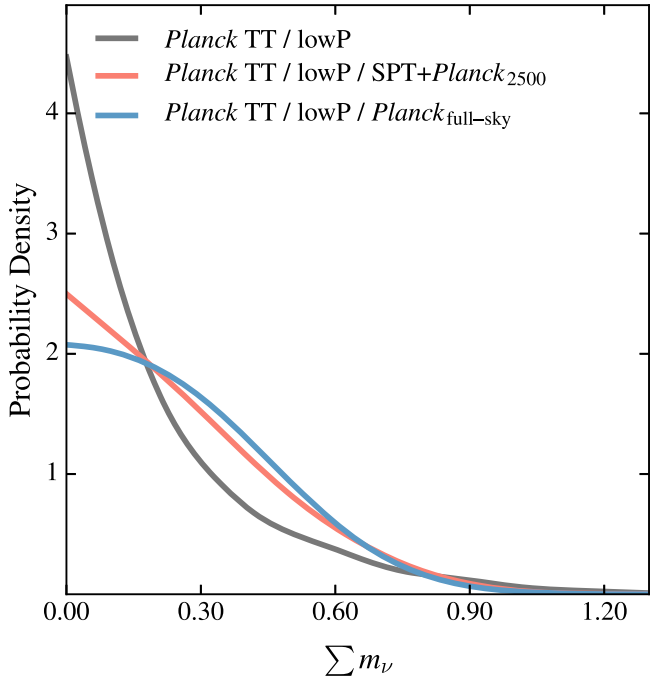

Figure 7. Limits on neutrino masses, showing *Planck* power spectrum information on its own (gray), and adding either *Planck* lensing data (blue) or SPT + *Planck* information (red).

Using SPT + *Planck*, the upper limit on neutrino masses is $M_\nu < 0.70$ eV at 95% confidence, compared to $M_\nu < 0.68$ eV for adding *Planck* full-sky lensing reconstruction data.

6. Discussion

The SPT + *Planck* data are not quite as constraining as the *Planck*-only lensing constraints; while the signal-to-noise per pixel of the O17 lensing map is substantially higher, the combined map covers only 2500 deg^2. As discussed in O17, the statistical precision of the combined lensing map is dominated by the SPT data. This measurement is therefore a nearly independent check on the *Planck* lensing measurement.

The SPT + *Planck* lensing measurements and resulting cosmological constraints are in close agreement with the full-sky lensing results of the *Planck* experiment. For example, the SPT + *Planck* lensing measurements are in excellent agreement with a spatially flat universe, as predicted by inflationary models, with $\Omega_k = -0.012^{+0.021}_{-0.023}$ at 95% confidence, while a constraint on local structure from SPT + *Planck* is $\sigma_8\Omega_{\rm m}^{0.25} = 0.601 \pm 0.023$. Using *Planck* lensing instead yields $\Omega_k = -0.005^{+0.016}_{-0.017}$ and $\sigma_8\Omega_{\rm m}^{0.25} = 0.607 \pm 0.015$. These new measurements are nearly statistically independent of the *Planck*-only results, so the agreement between the data sets is informative.

This trend is also true for slight tensions that exist in *Planck* between the amount of lensing inferred from peak smearing and the direct reconstructions from the higher-order statistics. Measurements of the lensing amplitude from SPT + *Planck* are in excellent agreement with the lensing amplitude inferred from the *Planck* higher-order statistics, and in slight tension with that inferred from CMB peak smearing. When marginalizing over the peak smearing effect, the SPT + *Planck* data are in close agreement with the expected amount of gravitational lensing otherwise predicted by the observed CMB fluctuations.

The amount of lensing seen in SPT + *Planck* is also broadly consistent with both the amplitude inferred from low-redshift galaxy lensing studies and the amplitude of structure inferred from the *Planck* primary CMB measurements, as was also the case with *Planck*-only lensing constraints. More precise CMB lensing measurements will be required to further investigate possible tensions between low-redshift and high-redshift determinations of the amplitude of structure.

G.S. wishes to thank Elisa GM Ferreira, Joachim Harnois-Déraps and Alexander van Engelen for useful discussions and Jack Holder for digitization of the foreground model. We acknowledge the use of Alexander van Engelen's implementation of the analytical $N_L^{(1)}$ bias in the flat-sky approximation. The South Pole Telescope program is supported by the National Science Foundation through grant PLR-1248097. Partial support is also provided by the NSF Physics Frontier Center grant PHY-0114422 to the Kavli Institute of Cosmological Physics at the University of Chicago, the Kavli Foundation, and the Gordon and Betty Moore Foundation through Grant GBMF#947 to the University of Chicago. This work has made use of computations performed on Guillimin, managed by Calcul Quebec and Compute Canada (funded by CFI, MESI, and FRQNT), and the Blue Waters sustained-petascale computing project (supported by NSF awards OCI-0725070 and ACI-1238993 and the state of Illinois). The McGill authors acknowledge funding from the Natural Sciences and Engineering Research Council of Canada, Canadian Institute for Advanced Research, and Canada Research Chairs program. G.S. acknowledges support from the Fonds de recherche du Québec—Nature et technologies. B.B. has been supported by the Fermi Research Alliance, LLC under Contract No. DE-AC02-07CH11359 with the U.S. Department of Energy, Office of Science, Office of High Energy Physics. C.R. acknowledges support from Australian Research Councils Discovery Projects scheme (DP150103208). Work at Argonne National Laboratory was supported under U.S. Department of Energy contract DE-AC02-06CH11357.

ORCID iDs

G. Simard https://orcid.org/0000-0001-5800-3990
Y. Omori https://orcid.org/0000-0002-0963-7310
E. J. Baxter https://orcid.org/0000-0002-6836-3196
R. Chown https://orcid.org/0000-0001-8241-7704
T. M. Crawford https://orcid.org/0000-0001-9000-5013
T. de Haan https://orcid.org/0000-0001-5105-9473
E. M. George https://orcid.org/0000-0001-7874-0445
G. P. Holder https://orcid.org/0000-0002-0463-6394
A. Manzotti https://orcid.org/0000-0003-0057-877X
C. L. Reichardt https://orcid.org/0000-0003-2226-9169
A. A. Stark https://orcid.org/0000-0002-2718-9996
J. D. Vieira https://orcid.org/0000-0001-7192-3871
W. L. K. Wu https://orcid.org/0000-0001-5411-6920

References

Abazajian, K. N., Arnold, K., Austermann, J., et al. 2015, APh, 63, 66
BICEP2 Collaboration, Keck Array Collaboration, Ade, P. A. R., et al. 2016, ApJ, 833, 228
Böhm, V., Schmittfull, M., & Sherwin, B. D. 2016, PhRvD, 94, 043519
Challinor, A., & Lewis, A. 2005, PhRvD, 71, 103010
Chon, G., Challinor, A., Prunet, S., Hivon, E., & Szapudi, I. 2004, MNRAS, 350, 914
Christensen, N., Meyer, R., Knox, L., & Luey, B. 2001, CQGra, 18, 2677
Das, S., Marriage, T. A., Ade, P. A. R., et al. 2011a, ApJ, 729, 62
Das, S., Sherwin, B. D., Aguirre, P., et al. 2011b, PhRvL, 107, 021301
Hanson, D., Challinor, A., Efstathiou, G., & Bielewicz, P. 2011, PhRvD, 83, 043005
Henning, J. W., Sayre, J. T., Reichardt, C. L., et al. 2018, ApJ, 852, 97
Hildebrandt, H., Viola, M., Heymans, C., et al. 2017, MNRAS, 465, 1454
Hu, W., & Okamoto, T. 2002, ApJ, 574, 566
Joudaki, S., Blake, C., Heymans, C., et al. 2017, MNRAS, 465, 2033
Keisler, R., Reichardt, C. L., Aird, K. A., et al. 2011, ApJ, 743, 28
Kesden, M., Cooray, A., & Kamionkowski, M. 2003, PhRvD, 67, 123507
Komatsu, E., Smith, K. M., Dunkley, J., et al. 2011, ApJS, 192, 18
Lewis, A., & Bridle, S. 2002, PhRvD, 66, 103511
Lewis, A., & Challinor, A. 2006, PhR, 429, 1
Lewis, A., Challinor, A., & Lasenby, A. 2000, ApJ, 538, 473
Namikawa, T., Hanson, D., & Takahashi, R. 2013, MNRAS, 431, 609
Okamoto, T., & Hu, W. 2003, PhRvD, 67, 083002
Omori, Y., Chown, R., Simard, G., et al. 2017, ApJ, 849, 124
Planck Collaboration 2014a, A&A, 571, A16
Planck Collaboration 2014b, A&A, 571, A17
Planck Collaboration 2016a, A&A, 594, A13
Planck Collaboration 2016b, A&A, 594, A15
POLARBEAR Collaboration 2014, PhRvL, 113, 021301
Schmittfull, M. M., Challinor, A., Hanson, D., & Lewis, A. 2013, PhRvD, 88, 063012
Sherwin, B. D., Dunkley, J., Das, S., et al. 2011, PhRvL, 107, 021302
Sherwin, B. D., van Engelen, A., Sehgal, N., et al. 2017, PhRvD, 95, 123529
Smith, K. M., Hu, W., & Kaplinghat, M. 2006, PhRvD, 74, 123002
Smith, K. M., Zahn, O., & Doré, O. 2007, PhRvD, 76, 043510
Stompor, R., & Efstathiou, G. 1999, MNRAS, 302, 735
Story, K. T., Hanson, D., Ade, P. A. R., et al. 2015, ApJ, 810, 50
Story, K. T., Reichardt, C. L., Hou, Z., et al. 2013, ApJ, 779, 86
Szapudi, I., Prunet, S., Pogosyan, D., Szalay, A. S., & Bond, J. R. 2001, ApJL, 548, L115
Troxel, M. A., MacCrann, N., Zuntz, J., et al. 2017, arXiv:1708.01538
van Engelen, A., Bhattacharya, S., Sehgal, N., Holder, G. P., Zahn, O., & Nagai, D. 2014, ApJ, 786, 13
van Engelen, A., Keisler, R., Zahn, O., et al. 2012, ApJ, 756, 142
Zaldarriaga, M., & Seljak, U. 1999, PhRvD, 59, 123507